Efficient generation of collimated frequency upconversion blue light in rubidium vapor

Rui Cao (曹 睿)[1,2], Baodong Gai (盖宝栋)[2], Jie Yang (杨 杰)[1,2], Tong Liu (刘 通)[2], Jinbo Liu (刘金波)[2], Shu Hu (胡 墅)[2], Jingwei Guo (郭敬为)[2,*], Yannan Tan (谭彦楠)[2], Shan He (何 山)[2], Wanfa Liu (刘万发)[2], Hongxing Cai (蔡红星)[1], and Xihe Zhang (张喜和)[1]

[1]*School of Science, Changchun University of Science and Technology, Changchun 130022, China*
[2]*Key Laboratory of Chemical Lasers, Dalian Institute of Chemical Physics, Chinese Academy of Science, Dalian 116023, China*
**Corresponding author: jingweiguo@dicp.ac.cn*

Received September 1, 2015; accepted October 27, 2015; posted online December 18, 2015

Pulsed collimated blue light at 420.3 nm is generated in hot Rb vapor by upconverting the 778.10 nm pumping beam through four wave mixing process. The energy conversion efficiency exceeds 1% when a 45 cm-long, 170°C heated Rb cell is used. The influence of cell temperature, wavelength, and energy of a pumping laser are fully examined. The efficiency of the photon conversion is found to be more sensitive to the blue detuning of the pump light and less sensitive to the red detuning of the pump light. This phenomenon can be explained by stimulated hyper-Raman scattering involved in the four-wave mixing process.

OCIS codes: 190.4380, 190.4180, 190.7220, 300.6210.
doi: 10.3788/COL201513.121903.

A blue (400–500 nm) laser has very important applications in underwater optical communication for its low absorption coefficient in water[1]. Also, the blue band is admirable in materials processing and information storage for its short wavelength. The generation of 420 nm blue light from Rb vapor has attracted more interest since the first report of blue light from pumping Rb vapor with a mixture of laser wavelengths of 780 and 776 nm, in 2002[2]. However, improving the power conversion efficiency is still a challenge. 1.1 mW cw 420 nm light with a conversion efficiency of 2.6% was realized in 10^{-3} mbar Rb in 2010[3], then 9.1 mW cw 420 nm light with a power efficiency of 1.5% was successfully achieved in 2014[4]. Single-wavelength conversion using 778 nm has also been realized[5]. Pulsed 420 nm light was also reported[6], with single-wavelength 778.1 nm pumping; the slope efficiency was 0.5% and the power efficiency reached about 0.5%. This is the highest power efficiency record for similar pulsed laser frequency upconversion.

Although the linewidth of a dye laser is usually several GHz, which does not match the atom absorption well, a pulsed nanosecond dye laser has a much higher peak power in comparison with cw-laser diodes. Therefore, the probability for non-resonant two-photon excitation will increase dramatically. In this work, a 45 cm-long, 170°C heated Rb vapor cell was used, 420 nm pulsed blue light with energy efficiency over than 1% was generated by a pulsed dye laser with a linewidth of 3 GHz. A conversion mechanism including hyper-Raman and four-wave mixing (FWM) is given for the explanation of experimental results.

The Rb cell used in this work was homemade with quartz glass. The filling process was completed in a vacuum glove box under the protection of pure helium. The concentrations of water vapor and oxygen were controlled under 1 ppm. After the filling, the Rb cell was pumped to a vacuum of 0.1 Torr by a rotary pump, and the opening was sealed by heating. Rb metal of natural isotope distribution was used. A frequency-doubled *Q*-switched Nd:YAG with a repetition rate of 10 Hz was used to pump a dye laser (Continuum ND6000). Laser dye styryl8 dissolved in dimethylsulfoxide was used to generate the pump laser of 778.1 nm. The wavelength of the dye laser was monitored by a wavelength meter with an accuracy of ±600 MHz. Lasers out of the Rb cell were diffracted by a grating with a known diffracting efficiency to separate the blue-light and residual-pumping laser. The laser power was recorded by mJ- or μJ-grade pyroelectric detectors. Spectra of blue light were recorded by a fiber-coupled CCD spectrometer. Different cell temperatures from 130°C to 280°C were tried for highest conversion efficiency. The dye laser was restricted to a diameter of 1.5 mm by an iris to gain a near-flattop beam through experiments for consistency.

By monitoring the blue light energy while scanning the wavelength of the dye laser, 778.10 nm is found to be the optimized wavelength for generating 420 nm blue light (two-photon excitation from the $5^2S_{1/2}$ to the $5^2D_{5/2}$ state). At a pump energy of ~0.85 mJ/pulse, a reproducible high efficiency of blue light appears at about 170°C when changing the cell temperature. Lower temperatures lead to low efficiency and higher temperatures can cause fast cell damage.

Figure 1 shows the pulse energy of the output blue light versus temperature and atom density[7]; here, the optimized pumping wavelength of 778.10 nm is used. The wavelength of the blue light is measured to be 420.3 nm. The data points in Fig. 1 show a logarithm tendency,

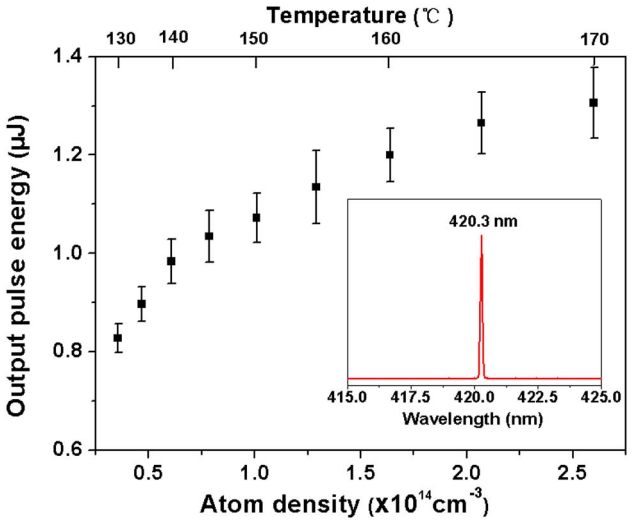

Fig. 1. Blue light energy versus the Rb atom density and the corresponding temperature of the Rb cell, measured with a fixed pumping energy. The inset is a spectrum of the blue light. The pumping-pulse energy used here is about 0.85 mJ. The blue light is separated from the residual pump light with a grating for measuring the pulse energy; the collecting efficiency for light of 420 nm is not optimized.

which means by increasing atom density the blue light energy and the corresponding conversion efficiency go higher; however, the growth speed is slower than a linear growth.

For getting as high of a blue light efficiency as possible, the cell temperature is fixed to 170°C and the pumping wavelength is fixed to 778.10 nm. After efforts on improving cell manufacturing, the energy of the blue output and the conversion efficiency are given in Fig. 2. The energy efficiency is 0.58%–1.74%. When the pulse energy of the dye laser is less than 0.5 mJ, the energy efficiency is higher than 1%. For a simple calculation, the pumping volume in the cell is about 0.80 cm^3, containing 2.1×10^{14} Rb atoms. Assuming that one atom absorbs 2 photons, the corresponding absorbed laser energy should be 0.10 mJ. Since the absorption is observed to be descending with the ascending pumping energy, the descending efficiency in Fig. 2 is believed to be mainly related to the very high pumping energy. For example, when the pumping pulse is about 1.5 mJ the absorption is lower than the energy fluctuation of the pumping laser and cannot be determined. Slight "fogging" is observed on both windows of the Rb cell after ten h of heating at 170°C; if it can be avoided, the efficiency would be further improved. Each point in Fig. 2 is the average of 1500 pulses; there is still a slight fluctuation in the curves. The fluctuation is quite possibly derived from changes in the surrounding environment such as instability of temperature, cell fading, or a slow changing of the dye laser pointing direction.

Figure 3 shows the intensity profile of the blue light as the pumping laser is detuned from 778.10 nm. The intensity profile shows wide asymmetric wings. This phenomenon has not been reported by others. The red wing is spreading more than the blue wing, and a shoulder peak exists in the red side. When the pyroelectric detector is replaced by a spectrometer, two blue wavelengths, 420.3 and 421.7 nm, are observed and are shown in Fig. 4. They correspond to the $6^2P_{3/2} - 5^2S_{1/2}$ and $6^2P_{1/2} - 5^2S_{1/2}$ transitions in the Rb atom. Two wavelengths have similar wings to Fig. 3. Though larger fluctuations exist in spectroscopy, asymmetric wings can be clearly observed.

Figure 5 is the recorded absorption curve with wavelength scanning. A broad asymmetric absorption peak is observed. Under these experimental conditions Rb atoms are expected to show Doppler broadened absorption with a linewidth of about 1 GHz. Therefore, the much broader absorption peaks must represent kinds of nonlinear absorption.

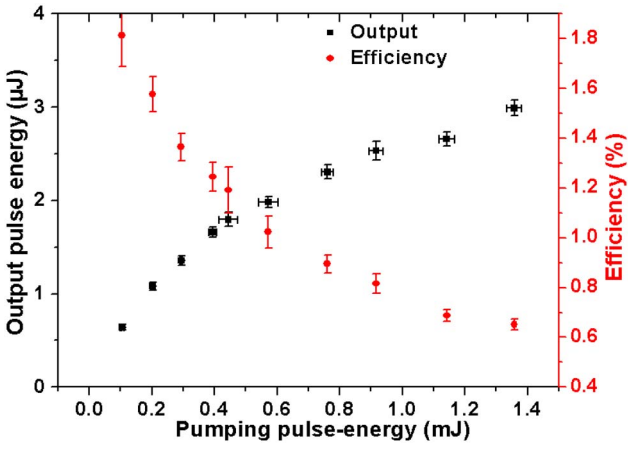

Fig. 2. Pulse energy and conversion efficiency of blue light versus the pumping pulse energy. Noting that the pump and output pulse energies are raw data, the transmission loss of the uncoated window (8%) and the diffraction efficiency of the grating (40%) are considered when calculating the efficiency.

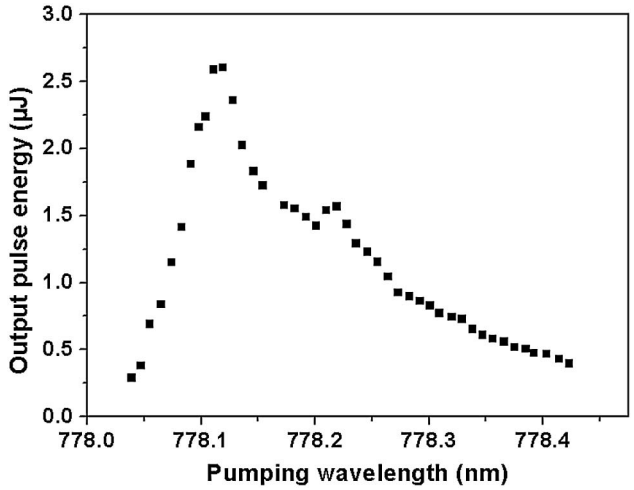

Fig. 3. Pulse energy of the blue light versus pumping wavelength (recorded by energy meter). Pumping energy is stable when scanning the wavelength.

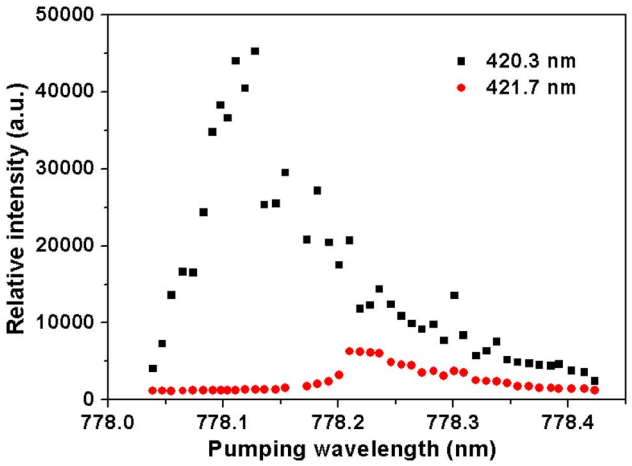

Fig. 4. Relative intensities of 420.3 and 421.7 nm blue lights versus pumping wavelength. Spectra were collected with a fiber-coupled spectrometer. The fiber cannot collect the whole blue spot like the pyroelectric detector used in Fig. 3, so larger fluctuations appear on curves in Fig. 4 than in Fig. 3.

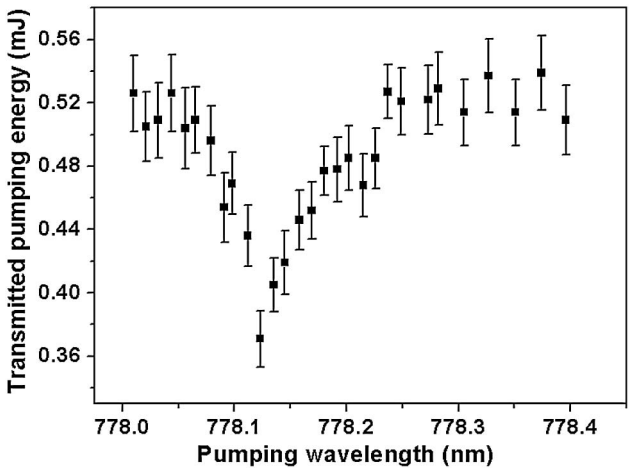

Fig. 5. Typical two-photon absorption profile of Rb vapor. The pumping energy is stable when scanning the wavelength and the curve shows a decreased energy of output pulses when absorption happens.

The most widely accepted mechanism for blue light generation from Rb vapor under 780 + 776 nm, or single 778 nm pumping is FWM, but not a direct one. Taking the 778 nm as an example, Rb atoms can be excited to the $5^2D_{5/2}$ energy level by absorbing two 778 nm photons. The lower $6^2P_{3/2}$ level is not populated at first, so population inversion will form between the $5^2D_{5/2}$ level and the lower $6^2P_{3/2}$ level. When the population inversion is large enough, an amplified spontaneous emission (ASE) of 5.233 μm is generated. Finally, resonating FWM with 778 nm and 5.233 μm happens to generate 420.3 nm forward-going light resonating with the transition from $6^2P_{3/2}$ to $5^2S_{1/2}$[8]. Degenerate two-photon absorption can be expressed with the formula

$$\frac{dI}{dx} = -N_{\mathrm{Rb}} \cdot \sigma_{2\mathrm{photon}} \cdot I^2, \tag{1}$$

where I is the light intensity, x is the distance, N_{Rb} is the Rb atom density, and the Doppler free two-photon absorption cross sections $\sigma_{2\mathrm{photon}} = 1.2 \times 10^{18}$ cm^4 · W^{-1} from Ref. [6]. By integrating Eq. (1) we get:

$$\frac{1}{I_0} - \frac{1}{I_l} = -N_{\mathrm{Rb}} \cdot \sigma_{2\mathrm{photon}} \cdot l, \tag{2}$$

where l represents the cell length and its value is 45 cm. In Fig. 5, the max absorption results in a residual of 0.371 mJ from the original ~0.526 mJ in the experiment (pumping laser with an spot diameter of 1.5 mm and an FWHM pulse duration of 5 ns). Here, $N_{\mathrm{Rb}} = 2.60 \times 10^{14}$ cm^{-3}. The nominal $\sigma_{2\mathrm{photon}}$ is calculated to be 6.0×10^{-24} cm^4 W^{-1} for this experiment, which is much smaller than the expected value. The pumping laser linewidth is probably one reason responsible for this discrepancy. The factory-measured dye laser linewidth is 3 GHz (0.1 cm^{-1}), 3 times that of the Doppler-broadened atom line.

However, the two-photon absorption cannot explain everything, especially the allowed large tuning range in Figs. 3 and 4 and the broad absorption band in Fig. 5. These remind us of the possibility of stimulated hyper-Raman scattering[9]. Atoms can absorb two photons simultaneously, then hyper-Raman scattering happens, generating directional infrared radiation just like the ASE from the transition from $5^2D_{5/2}$ to $6^2P_{3/2}$. But there is a large difference between hyper-Raman and ASE. Hyper-Raman radiation has variable Stokes wavelengths with the following wave frequency:

$$2h\nu_{\mathrm{pump}} - h\nu_{\mathrm{stokes}} = E_{6^2P_{3/2,1/2} \to 5^2S_{1/2}}. \tag{3}$$

The gain factor for stimulated hyper-Raman scattering can be expressed as[10,11]

$$G = \frac{N_{\mathrm{Rb}} I^2 \omega_s e^6}{30\hbar^5 (5\varepsilon_0 c)^3 \Gamma} \cdot \left\{ \frac{\langle 6p|r|5d\rangle \langle 5d|r|5p\rangle \langle 5p|r|5s\rangle}{\Delta\omega_1 \Delta\omega_2} \right\}^2 \cdot K\Theta, \tag{4}$$

where $\Delta\omega_1$ is $(\omega_{5^2P_J - 5^2S_{1/2}} - \omega_{\mathrm{pump}} + i\gamma_1)$, $\Delta\omega_2$ is $(\omega_{5^2D_J - 5^2S_{1/2}} - 2\omega_{\mathrm{pump}} + i\gamma_2)$, γ stands for the damping coefficient related to the atom life, N_{Rb} is the Rb atom volume density, Θ is the constant related to the pumping polarization and the Stokes wave propagating direction, K is a constant related to the degenerate levels, and the $\langle i|r|j\rangle$s stand for the transition dipole moments.

Hyper-Raman scattering happens between atom energy levels and "virtual energy levels." A virtual energy level is statistical combination of real energy levels. Being nearer to real levels, a virtual level gives larger hyper-Raman transition possibility. For this work, asymmetric peaks in Figs. 3 and 4 are inferred, deriving partly from the asymmetric efficiency-to-wavelength curve of stimulated hyper-Raman scattering, since the pumping photon (778.10 nm) energy is slightly higher than the energy

for the 5^2P_J to ground state (780 and 795 nm). Transition of the 5^2P_J to ground state has the largest transition dipole moment in Rb atom transitions, and the energy divergence of a pumping photon to 5^2P_J is apparently not symmetric in the tuning range. Finally, the asymmetric divergence contributes to the asymmetric stimulated hyper-Raman gain G in Eq. (4) and the asymmetric Stokes beam strength. The FWM efficiency is also affected by the resonating degree of the mixing waves with real energy levels just like Eq. (4). An asymmetric FWM efficiency-to-wavelength curve is believed to be another reason for asymmetric wings in Figs. 3 and 4.

Finally, as an explanation, FWM (generating 420.3 or 421.7 nm blue light, or generating them simultaneously) happens with three waves, including two degenerate waves around 778 nm and a mid-infrared beam. The mid-infrared beam is generated from ASE or stimulated hyper-Raman scattering. Hyper-Raman scattering is generally suppressed at the wavelength exactly resonating with transitions to certain energy levels, forming a dip in the curve shape of the Stokes output versus the pumping wavelength[10,12,13]. ASE at 5.233 μm derives from two-photon absorption at the pumping wavelength; resonating $5^2D_{5/2}$ (778.10 nm) is believed to contribute mostly to the peak tips in Figs. 3 and 4, instead of forming a dip. A wavelength-scanning result related to the two-photon absorption process and ASE is given in Ref. [5]. Since quartz glass is not transparent for infrared light around 5.2 μm, the ∼5.2 μm beam could not be measured in the experiment. In all tests, the blue light has an identical polarization direction with the pumping laser, and the blue light is only copropagating with the pumping laser. Such polarization and propagating make us believe that it comes from FWM. In all of the experiments, surprisingly the frequency upconversion did not show any fluctuation related to phase matching even at varying temperatures, though the vapor cell is 45 cm-long. One possible reason is the low dispersion of low-pressure Rb vapor. Furthermore, according to[10], hyper-Raman scattering has the property of giving a much broader Stokes linewidth than both the pumping linewidth and the Doppler-broadened atom linewidth. So another reason may be that the broad hyper-Raman Stokes line always covers the needed mid-infrared wavelength for an exact collinear phase-matching for FWM. An investigation of phase matching on the six-wave mixing process is given in Ref. [14], where the relative spectra-peak heights show a positive correlation with the phase matching. Further investigation is needed to elucidate the phase-matching mechanism.

In conclusion, high-efficiency generating of blue light is realized in Rb vapor. With a cell temperature of 170°C, a cell length of 45 cm, and a pumping laser energy less than 0.5 mJ/pulse, the conversion energy efficiency is larger than 1%. The upconversion is explained as two steps; (1) two-photon ASE or stimulated hyper-Raman scattering and (2) FWM.

This work was supported by the National Nature Science Foundation of China under Grant Nos. 61405197, 11304311, 11475177, and 61505210.

References

1. R. C. Smith and K. S. Baker, Appl. Opt. **20**, 177 (1981).
2. A. S. Zibrov, M. D. Lukin, L. Hollberg, and M. O. Scully, Phys. Rev. A **65**, 882 (2002).
3. A. Vernier, S. Franke-Arnold, E. Riis, and A. S. Arnold, Opt. Express **18**, 17020 (2010).
4. J. F. Sell, M. A. Gearba, B. D. DePaola, and R. J. Knize, Opt. Lett. **39**, 528 (2014).
5. E. Brekke and L. Alderson, Opt. Lett. **38**, 2147 (2013).
6. C. V. Sulham, G. A. Pitz, and G. P. Perram, Appl. Phys. B **101**, 57 (2010).
7. C. B. Alcock, V. P. Itkin, and M. K. Horrigan, Can. Metall. Q. **23**, 309 (1984).
8. A. Akulshin, D. Budker, and R. Mclean, Opt. Lett. **39**, 845 (2014).
9. P. P. Sorokin, J. J. Wynne, and J. R. Lankard, Appl. Phys. Lett. **22**, 342 (1973).
10. D. Cotter, D. C. Hanna, W. H. W. Tuttlebee, and M. A. Yuratich, Opt. Commun. **22**, 190 (1977).
11. Z. J. Jabbour, M. S. Malcuit, and J. Huennekens, Appl. Phys. B **52**, 281 (1991).
12. Y. P. Malakyan, Sov. J. Quantum Electron. **15**, 905 (1985).
13. J. Reif and H. Walther, Appl. Phys. **15**, 361 (1978).
14. C. J. Zhu, N. Tong, J. F. He, G. Q. Zhang, X. J. Zhai, and X. Bing, Chin. Phys. Lett. **31**, 88 (2014).